First-shell bond lengths in Si_xGe_{1-x} crystalline alloys

J. C. Aubry, T. Tyliszczak, and A. P. Hitchcock
Brockhouse Institute for Materials Research, McMaster University, Hamilton, Canada L8S 4M1

J.-M. Baribeau and T. E. Jackman
Institute for Microstructural Sciences, National Research Council, Ottawa, Canada
(Received 28 September 1998)

Si and Ge *K*-edge x-ray absorption fine structure (XAFS) spectra of strained and relaxed Si_xGe_{1-x} crystalline alloys grown by molecular beam epitaxy on Si(001) substrates are reported. For alloys with less than 30% Si, fluorescence yield detection is shown to be essential to avoid distortions of the Si *K*-edge XAFS signal caused by the underlying Ge *L*-edge XAFS signal from the majority Ge species. The average first shell structure has been deduced using simultaneous fitting of all data for relaxed alloys, while imposing physically reasonable constraints. The Ge-Ge, Ge-Si, and Si-Si first-shell distances are found to vary with composition. The results are compared with other experimental results and theoretical predictions in the literature. Our results are generally consistent with other experimental studies but they differ from recent theoretical predictions based on macroscopic elastic properties in that we observe a different compositional dependence [i.e., slope of $R(x)$ lines] for the Ge-Ge and Si-Si bond lengths. The slope for the Ge-Si bond length composition line was found to be intermediate between that of Si-Si and Ge-Ge. [S0163-1829(99)00316-1]

I. INTRODUCTION

In the last ten years, much interest has developed in crystalline Si-Ge alloys and heterostructures, in part because the intrinsic electronic properties of SiGe materials provide significant improvements in device properties with relatively simple incorporation into existing Si technology, and in part because of theoretical predictions that some strained SiGe materials might have a direct band gap and thus exhibit useful optoelectronic properties.[1–3] Silicon and germanium are fully miscible and form random substitutional alloys at all compositions.[4,5] The 4% difference in the lattice constants of Si and Ge produces significant strain during epitaxial growth of SiGe alloys. This changes the band structure relative to that of pure Si and Ge, and hence, changes the electronic properties,[6] creating the potential for band gap engineering in SiGe device technology. SiGe crystalline alloys are finding increasing uses, particularly in high-speed analog device technology.[7] SiGe device technology is in its infancy so further improvements are expected as growth and processing technologies mature. However, some fundamental questions are still unresolved: How does the local structure achieve strain accommodation? Which are the most important lattice relaxation modes? Are there conditions in which atomic ordering (compound formation) occurs?

Knowing the accurate local structure will help efforts to calculate the band structure of strained and relaxed SiGe alloys. Typically such calculations[6] use the virtual crystal approximation (VCA) for the structure of the SiGe unit cell. VCA, an extrapolation of Vegard's law to the structure of individual unit cells, assumes a linear dependence of bond length with composition.[8] For any given composition it assumes $R_{\text{Si-Si}}=R_{\text{Si-Ge}}=R_{\text{Ge-Ge}}$, and implies that bond lengths can distort to accommodate strain (i.e., R will be compositionally dependent), while bond angles are fixed at the tetrahedral angle. Even at the level of the lattice parameter, Vegard's law is never strictly obeyed. The lattice parameter of SiGe alloys has a slight negative deviation.[9] Much more of concern is the basic assumption of the VCA that the *local bonds* are directly related to the average unit cell structure. An alternate approximation is the Pauling model[10] in which the bond length between a given atom pair is fixed, independent of composition. In this limit the steric strain in alloys is accommodated by bond angle changes. Pauling's model is better suited for situations of directed chemical bonds, and thus it is probably a better zeroth order description of bonding in semiconductors, since these are highly covalent.

The virtual crystal approximation is a limitation of most alloy band-structure calculations; one expects more accurate band structures would result if an accurate structure is used. Unfortunately, despite considerable research, the *local* structure of crystalline SiGe alloys is still in question. In this work we use high-precision XAFS (extended x-ray absorption fine structure) spectroscopy[11,12] measurements to determine the nearest-neighbor atom pair distances as a function of alloy composition. The main thrust of this paper is the investigation of the thermodynamic limit in the form of *relaxed* SiGe alloys. However, results for some *strained* samples are also presented.

A. Review of theoretical models for the Si-Ge alloy local structure

There have been a number of *theoretical studies* of the local structure of SiGe alloys. Martins and Zunger[8] calculated Si-Ge bond lengths at the impurity limits and estimated $\mathbf{r}_{\text{SiGe}}=2.419$ Å for Si in *c*-Ge and $\mathbf{r}_{\text{GeSi}}=2.380$ Å for Ge in *c*-Si. Ichimura *et al.*,[13] using a zinc-blende structure of SiGe as a model of random SiGe alloys, predict that the three nearest-neighbor bond lengths have a linear dependence on

composition. The results of de Gironcoli *et al.*[14] and Weidmann and Newman[15] are similar.

Simplified models of the compositional dependence of the first-shell distances, based on macroscopic elastic properties, have also been proposed. Thorpe and co-workers,[16–18] using the Kirkwood model harmonic interatomic potential,[19] have defined a *topological rigidity parameter*, $\mathbf{a}^{**} = u_{AB}\alpha/F_{radial}$, that describes the resistance of a given lattice to a radial expansion from a central atom. Here, $\mathbf{F}_{radial}$ is the radial force from the central atom pushing away a nearest-neighbor atom, α_{AB} is the radial force constant for the *AB* bond, and $\mathbf{u}_{AB}$ is the displacement of the nearest-neighbor atom relative to its natural bond length. When $\mathbf{a}^{**}=1$, the lattice is ''floppy,'' every bond adopts its natural length, and the system is at the Pauling limit. When $\mathbf{a}^{**}=0$ the lattice is perfectly rigid, every bond extends or contracts to fit within the rigid unit cell defined by the lattice parameter, and the system is at the Vegard limit. Intermediate values of $\mathbf{a}^{**}$ describe mixed behavior. The parameter $\mathbf{a}^{**}$ depends on the ratios of the elastic linear and elastic shear force constants. Cai and Thorpe[16] showed that, using macroscopic elastic response, a^{**} can be described approximately by

$$a^{**}=[1+c_1(\beta/\alpha)]/[1+c_2(\beta/\alpha)+c_3(\beta/\alpha)^2],$$

where β is the angular elastic force constant, α is the linear elastic force constant, and c_1, c_2, and c_3 are constants. Based on the bulk elastic and shear modulii for pure Si and Ge, Thorpe *et al.* predicted that $\mathbf{a}^{**}$ is 0.707 for SiGe alloys.[20] This framework provides a method of relating the compositional dependence of nearest-neighbor bond lengths to the lattice rigidity, defined in terms of a single parameter $\mathbf{a}^{**}$. A consequence of the model is that the Si-Ge bond length of the 50% alloy must be 2.401 Å, regardless of the value of $\mathbf{a}^{**}$, and that a plot of the SiSi, SiGe, and GeGe bond lengths versus composition should consist of three equally spaced, parallel lines having a slope that is directly related to the value of $\mathbf{a}^{**}$. The prediction that the compositional dependence should have the form of three equally spaced, parallel lines is common to a number of semiempirical theoretical approaches.[13–15]

B. Review of experimental results for the Si-Ge alloy local structure

The *experimental* x-ray absorption fine structure (XAFS) *results* reported in the literature[21–33] differ qualitatively from the theoretical predictions. In contrast to the consistent theoretical picture of approximately 30% Vegard character, several XAFS studies on both amorphous and crystalline SiGe alloys have reported that the bonding in SiGe materials is essentially at the Pauling limit.[21–28] In a Ge *K* XAFS study of hydrogenated amorphous SiGe alloys (*a*-SiGe:H) Incocia *et al.*[21] reported $\mathbf{r}_{SiGe}=2.38$ Å independent of composition. Nishino *et al.*,[22] also using Ge *K*-edge XAFS, found that *a*-SiGe:H alloys are at the Pauling limit, with $\mathbf{r}_{GeGe}=2.460(5)$ Å and $\mathbf{r}_{SiGe}=2.410(5)$ Å. Filliponi *et al.*[23] made Si *K*-edge XAFS measurements of a similar series of *a*-SiGe:H alloys and found that $\mathbf{r}_{GeSi}=2.40(2)$ Å and $\mathbf{r}_{SiSi}=2.36(2)$ Å. Although the values differ, all three studies indicate that the bond lengths are essentially independent of composition.

The local structure of amorphous and crystalline alloys can differ significantly.[16–18] The disordered nature of amorphous materials implies the lattice is not rigid. This should provide greater opportunity to accommodate strain through bond-angle variation, and thus, bond lengths might be expected to be closer to their ''natural'' or Pauling-limit values in amorphous materials. Crystalline SiGe alloys have much less disorder than *a*-SiGe:H, as evidenced by their well-developed Si *K*-edge multiple scattering x-ray absorption near-edge structure which is a clear indicator of long-range ordering.[31–33] The more rigid lattice of a highly crystalline alloy could act as a stronger constraint on local bonding, forcing greater regularity in bond angles and thus some strain accommodation by bond-length variation. Thus results for amorphous *a*-SiGe:H alloys[21–23] may not be valid for crystalline SiGe alloys.

Recently, several studies of crystalline SiGe alloys have been reported. Matsuura *et al.*[24] measured Ge *K*-edge XAFS of a series of strained, Si rich (82%–94% Si) molecular-beam epitaxy (MBE)- and chemical vapor deposition (CVD)-grown SiGe crystalline epitaxial films and determined that $\mathbf{r}_{SiGe}=2.375(20)$ Å, independent of composition. While this is consistent with Pauling-type bonding, the magnitude of their error bars is much greater than any plausible compositional variation over such a small composition range.[24] Woicik *et al.*[25,26] performed Ge *K*-edge measurements of a strained epitaxial crystalline $Si_{.70}Ge_{.30}$ alloy grown by chemical vapor deposition (CVD) on Si(001). Single-shell filtered data was analyzed using *c*-Ge and GaP models to determine first-shell values of $\mathbf{r}_{GeGe}=2.44(2)$ Å, and $\mathbf{r}_{GeSi}=2.38(2)$ Å, very similar to the values in crystalline Ge (2.450 Å) and amorphous SiGe (2.38 Å) reported by Incocia *et al.*[21] Woicik *et al.*[26] have also reported polarization dependent XAFS of the same sample, allowing bond angles as well as first- and second-shell bond lengths to be determined. More recently, Woicik *et al.*[27] have examined the Ge *K*-edge XAFS of a series of three alloys (58%, 79%, and 90% Si). In this paper, they find a small but unequivocal variation in the Ge-Ge and Si-Ge bond lengths, which they interpret in terms of a model based on macroscopic elastic properties.

Kajiyama *et al.*,[28] using Ge *K*-edge XAFS, reported $\mathbf{r}_{Ge\text{-}Ge}=2.44$ Å and $\mathbf{r}_{GeSi}=2.40$ Å for materials they claim to be crystalline SiGe alloys spanning a range of compositions from 20–100 % Ge grown by CVD on polycrystalline graphite substrates. The Si-Ge and Ge-Ge first-shell bond lengths were found to be independent of alloy composition, indicating Pauling-type bonding in *c*-SiGe alloys. However, Mousseau *et al.*,[20] in a detailed reanalysis of the results of Kajiyama *et al.*[28] *based on the assumption that the topological rigidity model is applicable*, showed that strictly Pauling-type behavior would require unphysical elastic constants for Si-Ge bonding and that the Kajiyama *et al.* results could only be made compatible with the known lattice properties if the $\mathbf{r}_{SiSi}$ values (not measured by Kajiyama *et al.*) were 2.16–2.34 Å, far below that for *c*-Si (2.352 Å) and clearly unphysical. To account for this disagreement, Mousseau *et al.*[20] suggested that the Kajiyama *et al.* CVD samples were highly

TABLE I. Summary of Si_xGe_{1-x} crystalline alloy samples.

Code[a]	NRC#	% Si[b]	Substrate	d (nm)	Strain state	Lattice parameter (Å)
*G*5*s*	471	5	Ge	800	Strained	
*G*9*r*	425	9	Ge	750	Mostly relaxed	
*G*12*s*	423	12	Ge	550	Strained	
*G*20*s*	529	20	Ge	100	Strained	
*G*22*s*	686	22	Ge	25	Strained	
*S*29*r*	1475	29	Si	100	Relaxed	5.5909
*G*38*r*	1645	38	Ge	150	Relaxed	5.5658
*S*42*r*	1633	42	Si	250	Relaxed	5.5579
*S*56*r*	1201	56	Si	300	Relaxed	5.5298
*S*61*r*	1632	61	Si	250	Relaxed	5.5189
*S*78*r*	1478	78	Si	200	Relaxed	5.4798
*S*91*s*	1630	91	Si	500	Strained	5.4369
*S*99*s*	1064	99.2	Si	2000	Strained	-

[a]The first letter of this code refers to the substrate, the second and third numbers refer to the sample composition, and the fourth letter (*s*,*r*) refers to the strain state of the sample (strained or relaxed).

[b]The %Si is that determined from the measured lattice parameter using the literature values for the composition dependence (Ref. 9).

contaminated with hydrogen, in the form of large, planar hydride cracks within the polycrystalline films. However, the amount of hydrogen required (45-65 mol %) was quite high.

Following the Kajiyama and Mousseau dialog, Aldritch *et al.*[29] measured Ge *K*-edge XAFS of relaxed, MBE-grown epitaxial SiGe alloys. They reported for the first time, that the first-shell bond length of *c*-SiGe alloys has a detectable compositional dependence, and thus a partial Vegard-like character. In particular, although the results for the first-shell Si-Ge distance were rather ambiguous, the values for the first-shell Ge-Ge distance showed systematic compositional variation, which was in reasonable agreement with the theoretical predictions.[8,13–15,20] Based mainly on their Ge-Ge values, Aldrich *et al.*[29] determined $a^{**}=0.63(10)$, in good agreement with the values of a^{**} predicted from the theoretical work, which all lie between 0.6 and 0.7.[8,16–18,20]

We consider that the results of Woicik *et al.*[25–27] and Aldrich *et al.*[29] are very important, but insufficient to make a firm conclusion about the first-shell structure of relaxed, crystalline SiGe alloys. Specifically, in both cases the error bars on the first-shell distances are rather large and the conclusion is mainly based on the Ge-Ge distances, with contradictory trends from the Si-Ge distances, and no information about the Si-Si distances. Also, given the contradiction to the experimental results of Kajiyama *et al.*,[28] the Aldrich study[29] cannot be considered unambiguous evidence of non-Pauling behavior. Most significantly, the absence of Si *K*-edge data on the same samples does not permit the problem to be fully addressed. The discrepancies between some experimental results and the relatively large errors associated with all results are partly due to lack of an ideal empirical EXAFS standard for Si-Ge atom pairs,[27] as well as the fact that one has to deal with a mixed first coordination shell. In this paper, we have attempted to obtain the best possible quality Si and Ge *K*-edge XAFS spectra of a series of relaxed *c*-Si_xGe_{1-x} alloys grown by MBF on Si(001) and carry out a state-of-the-art XAFS analysis. Essentially the full compositional range ($x=0.05$ to 0.99) has been investigated. A simultaneous, multiedge, multispectrum, curve fitting methodology has been used to determine the first-shell bond lengths ($\mathbf{r}_{SiSi}$, $\mathbf{r}_{SiGe}$, and $\mathbf{r}_{GeGe}$) and coordination numbers, ($\mathbf{N}_{SiSi}$, $\mathbf{N}_{SiGe}$, $\mathbf{N}_{GeSi}$, and $\mathbf{N}_{GeGe}$), over the full range of composition.

II. EXPERIMENT

A. Samples

The *c*-SiGe alloy films were grown in a VG Semicon V80 molecular-beam epitaxy (MBE) system using solid Si and Ge sources, with electron beam evaporators. Base chamber pressure was typically $1-2*10^{-10}$ mbar, with an order of magnitude increase during growth. Samples were grown on commercial (100) oriented Si and Ge wafers. *Ex situ* wafer preparation consisted of 10 min in a UV/ozone reactor for hydrocarbon removal, followed by a 10-min *in situ* thermal oxide desorption process at 900 °C under a 0.01 nm/s Si flux on the Si wafer (600 °C for Ge, no flux). Typical growth temperatures were approximately 500 °C with a 0.2 nm/s flux rate for the Si and Ge beams. Source fluxes were measured and controlled by electron impact excitation spectroscopy monitors (Leybold, Sentinell III) calibrated against oscillating quartz microbalances. The fluxes were adjusted to achieve the desired compositions. The thickness of the relaxed samples was far beyond the maximum for coherent growth (see Table I). Estimates of the composition and strain in the samples were obtained by high-resolution x-ray diffraction using both symmetric (004) and asymmetric (224) scattering geometries. Except for one case (*S*91*s*) the samples were heavily relaxed (>75%) and the reported composition is that derived from the lattice parameter of the alloy layer,[9] taking into account residual tetragonal distortion of the lattice, rather than the nominal value from the MBE growth parameters.

B. XAFS measurements

Ge *K*-edge XAFS was measured at the C2 station at the Cornell High Energy Synchrotron Source (CHESS). Higher

harmonics were rejected by second crystal detuning. I_0 was measured using a gas ionization chamber. The total electron yield (TEY) signal from the sample was measured using a He gas ionization detector with sample rotation[34] to eliminate diffraction artifacts from the crystalline samples. The estimated TEY sampling depth at the Ge *K*-edge is 2000 Å.[35] Si *K*-edge XAFS was measured using both electron yield and fluorescence yield (FY) detection at the soft x-ray DCM line at the Canadian Synchrotron Radiation Facility at the Synchrotron Radiation Center (SRC) in Stoughton, Wisconsin. I_0 was measured with a N_2 gas cell enclosed by two Be windows (12.5 μm thickness). The energy scale linearity and accuracy was checked in each case. At CHESS, we used the Ge, Ga, and As *K*-edges while at SRC gas phase standards (SF_6, CH_3Cl, and Ar) were used. In the latter case, significant errors in energy scale were found, with an inaccuracy of up to 20 eV over 1000 eV. The linear energy scale correction that was applied was an important factor in achieving the quality of agreement between the Si-Ge distances derived simultaneously from Ge *K*-edge and Si *K*-edge data. All x-ray absorption data presented in this paper was acquired with the sample at ambient temperature (25–30 °C).

Even though the wavelength is quite long at the Si 1*s* edge (~6 Å) there is some diffraction from these near-perfect crystal samples and thus careful sample positioning was required to avoid sample diffraction artifacts (we note that in-vacuum sample rotation, as done at the Ge *K*-edge, would be a preferable solution). The samples were etched with hydrogen fluoride (10%) to remove surface oxide prior to measurement. This minimizes the surface work function and thus enhances electron yield, which is beneficial for both Si and Ge *K*-edge measurements. The etching is essential to eliminate spectral contamination from surface oxide, which can be significant since the estimated depth sensitivity for TEY at the Si *K*-edge is ~200 Å.

Initially all Si *K*-edge spectra were recorded by measuring the sample current, a variant of TEY detection. For the dilute Si_xGe_{1-x} alloys ($x<30\%$) the signal to background ratio is poor and very long signal integration combined with averaging was required to achieve adequate statistics. Much more seriously, the residual XAFS in the underlying Ge 2*p* continuum overwhelms the Si 1*s* XAFS for compositions below 20%. However, we were able to acquire the correct Si 1*s* signal for these samples by using fluorescence yield (FY) detection. Our first FY measurements detected the soft x-rays with a channelplate protected by a thin Al foil to eliminate interference from electron yield signals. Even though this approach does not separate Si 1*s* from Ge 2*p* fluorescence x-ray signal, the Ge 2*p* fluorescence yield is much weaker and thus most of the Ge 2*p* interference is removed. The data finally used for the dilute Si_xGe_{1-x} alloys ($x<30\%$) was acquired using a nine-element solid-state detector to isolate and record only the Si 1*s* fluorescence signal. Figure 1 compares the Si *K*-edge XAFS for a 9% Si alloy sample, detected by TEY and both types of FY. In addition to a much improved S: B, there is a dramatic difference in the extracted XAFS from TEY and FY (see lower panels in Fig. 1). In particular, the TEY XAFS is strongly distorted by a low-*R* signal, which is generated by the underlying Ge 2*p* XAFS, but analyzed using an inappropriate wave-number scale based on an incorrect edge position [1840 eV (Si 1*s*) rather than 1210 eV (Ge $2p_{3/2}$)]. Figure 2 compares the isolated XAFS and Fourier magnitude for the TEY signal with that extracted from experimental TEY measurements of pure *c*-Ge, and that predicted from FEFF 6.01 calculation,[36–38] in each case processed as Si 1*s* XAFS. From this comparison, as well as the difference in the TEY and FY results, it is clear that the low-*R* artifact arises from Ge 2*p* XAFS.

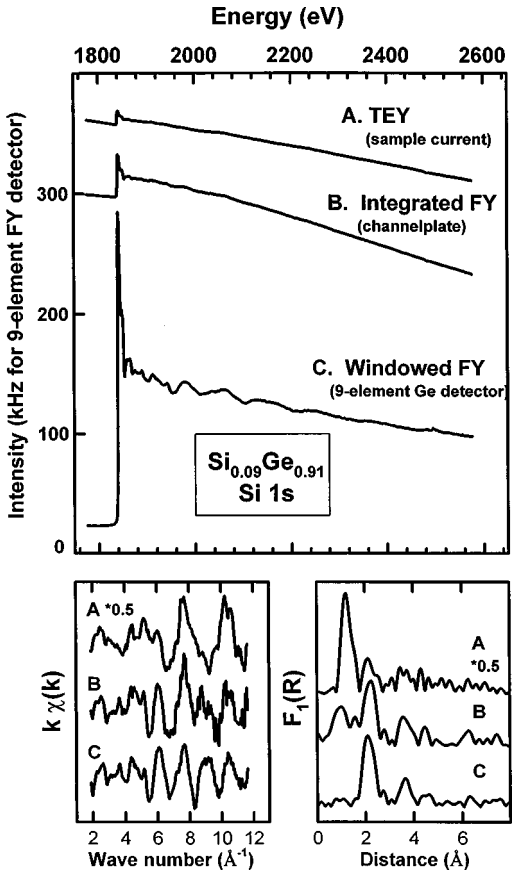

FIG. 1. As-recorded Si 1*s* XAFS signals from a 9% Si alloy recorded with (a) sample current (TEY), (b) integrated fluorescence using a shielded channel plate, and (c) a solid state nine-element array detector with electronic windowing of the Si K_α fluorescence. The true zero of each signal corresponds to the bottom of the plot window. The lower-left panel compares the $\chi(k)$ while the lower-right panel compares the magnitudes of the Fourier transforms of the XAFS signal extracted from the data shown in the main panel.

III. RESULTS

A. Data processing

A three-section cubic spline fit to the raw data in *k* space was used to remove the nonoscillatory background. The isolated XAFS was normalized to the intensity of the nonoscillatory continua, generated by subtracting the extrapolation of a linear fit to the pre-edge signal from a linear fit to the post-edge signal. This approach compensates for any systematic energy dependence of detector sensitivities such as photon-electron conversion ratios in TEY and window transmission in the FY detectors. The E_0, $k_{\min}$, and $k_{\max}$ values used to set the XAFS scales are reported in Table II. As far as possible, identical values

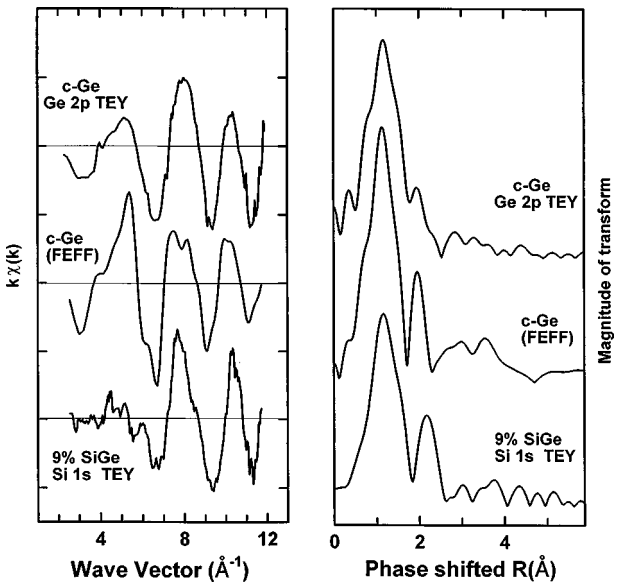

FIG. 2. Comparison of the $\chi(k)$ (left) and $F(R)$ (right) for experimental TEY signal from c-Ge (using 1840 as E_0); FEFF calculation; and the TEY from the 10% alloy. The artifact signal arises from the residual Ge $2p$ XAFS, even though the Si K-edge XAFS range (1855–2600 eV) corresponds to a rather high-k range of the Ge $2p$ XAFS ($13<k<19\,\text{Å}^{-1}$) using $E_0=1215$ eV, which is the correct value for Ge $2p$ signals). In part this artifact is large because the amplitude for Ge backscattering peaks at large k, in part because there is an order of magnitude more Ge than Si in this alloy.

were used for each data file to maximize reproducibility. Figure 3 depicts the Ge K-shell XAFS $[k^1.\chi(\mathbf{k})]$ (left panel) and magnitude of the Fourier transform $[\mathbf{F}_1(\mathbf{r})]$ (right panel) as a function of composition of the SiGe alloys as well as c-Ge. Figure 4 presents Si K-shell XAFS $[k^1.\chi(\mathbf{k})]$ and Fourier transforms $[\mathbf{F}_1(\mathbf{r})]$ for the SiGe alloys and for c-Si. The Fourier transform (FT) for the pure materials has a sharp, nearly symmetric first-shell signal and significant signal strength in the higher shells between 3–5 Å. In contrast, the FT of the alloys has a broader and asymmetric first-shell signal and only the alloys close to the pure materials exhibit defined peaks above 3 Å, beyond the first-shell structure.

TABLE II. Summary of XAFS analysis parameters. All transforms were carried out after zero-filling to 40 Å (reverse) or 40 Å^{-1} (forward).

Parameter	Ge K-edge	Si K-edge
$E_0(GG)$[a] (eV)	6.7	
$E_0(SG)$[a] (eV)	6.9	7.4
$E_0(SS)$[a] (eV)		7.3
k-min (Å^{-1})	3.3	3.3
k-max (Å^{-1})	end of data (~16)	end of data (~14)
k-weighting	1	1
R-min (Å)	0.8	0.8
R-max (Å)	2.8	2.8
Apodization	Hanning, 30%	Hanning, 30%

[a]Initial k-scales were set to the mid point of the edge jump as determined by differentiation.

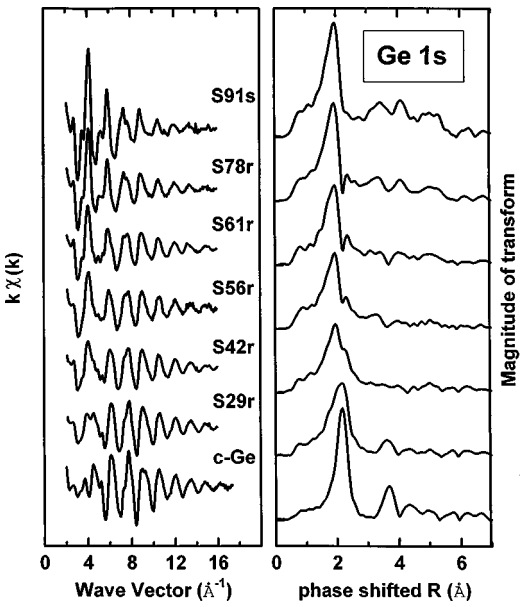

FIG. 3. (Left) $\chi(k)$ for Ge 1s XAFS of c-Ge and c-SiGe alloys (all relaxed, except 91%). (Right) Magnitude of the Fourier transform of the Ge 1s XAFS. All curves are on the same vertical scale, with offsets for clarity.

These aspects qualitatively indicate the random substitutional character of the structure, and they indicate the structure must be much closer to the Pauling that the Vegard limit, since well-defined higher shell signal would otherwise be observed from these crystalline alloys. The distorted first-shell peak shape, which typically has a long low-R shoulder and a sharp ''cut off'' on the high-energy side, is the manifestation of the beating between the two closely spaced first-shell components.

The first-shell signal (0.8–2.8 Å) of each transform was extracted, apodized, and then reverse Fourier transformed to

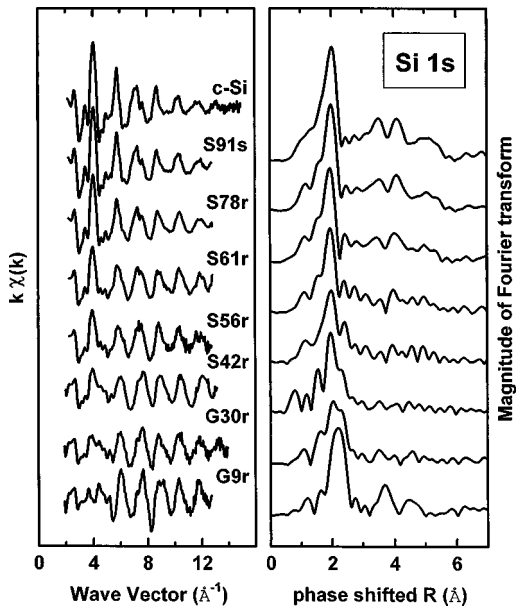

FIG. 4. (Left) $\chi(k)$ for Si 1s XAFS of c-Si and c-SiGe alloys (allrelaxed, except 91%). (Right) Magnitude of the Fourier transform of the Si 1s XAFS. All curves are on the same vertical scale, with offsets for clarity.

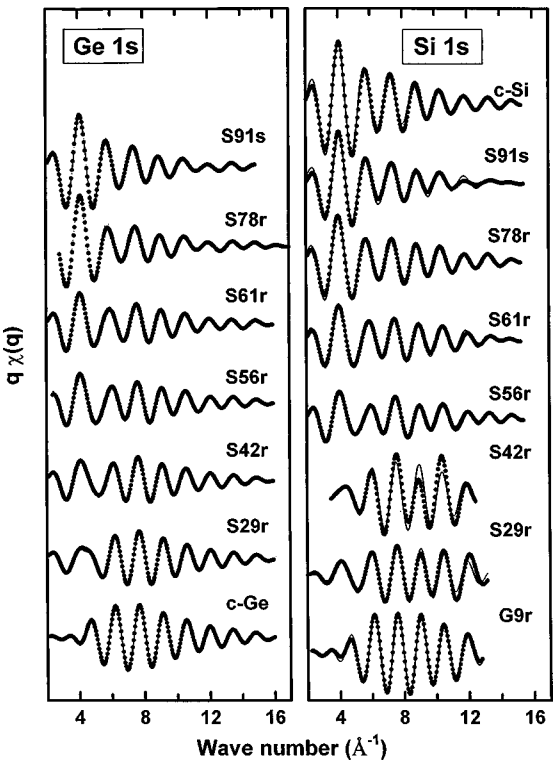

FIG. 5. (Left) Comparison of $\chi(q)$ Fourier-filtered first-shell Ge 1*s* XAFS with that from Feffit analysis. (Right) Comparison of $\chi(q)$ Fourier-filtered first-shell Si 1*s* XAFS with that from Feffit analysis. Dots, Fourier filtered experimental data; line fit.

isolate the first-shell signal in *k* space (Fig. 5; see Table II for details of the transform parameters). This signal was used as the input to the constrained, simultaneous multifile fit procedure. In order to extract quantitative information from the filtered first-shell XAFS, suitable models for the amplitude and phase are needed.[11,12] A number of different choices of models for the Si-Si, Si-Ge, Ge-Si, and Ge-Ge pairs were explored. These included experimental models-Ge *K* XAFS of *c*-Ge (Ge-Ge), Si *K* XAFS of *c*-Si (Si-Si), Ga *K* XAFS of GaP (Ge-Si), and P *K* XAFS of GaP (Si-Ge); FEFF-corrected experimental XAFS of GaP (to compensate for inappropriate *Z*); and fully theoretical models. (Recently, Woicik *et al.*[27] have shown that use of the average of experimental data for $(Z-1)$ and $(Z+1)$ systems is an effective approach.) In addition several different software packages were explored. The results presented here are based on the Feffit program,[38] which uses model phases and amplitudes calculated using FEFF 6.01.[36,37] Feffit allows optimization of the structural parameters with considerable flexibility in terms of imposing physically reasonable constraints to the parameter variance. It also provides statistical evaluation of errors, including estimations of parameter correlations.

XAFS is well known to be an ill-conditioned inversion problem so that fitting can give physically unreasonable results. Parameter correlation must be considered in evaluating fits. Various techniques are used to produce stable, meaningful results. One approach is to fit spectra from a series of similar samples and use the redundancy in the data set to reduce the number of degrees of freedom (fit parameters) by introduction of constraints appropriate to the problem. For example, all fits to the Ge *K*-edge spectra could be required to have the same values for the $\mathbf{E}_{0,\mathrm{GeGe}}$, implying a similar potential along Ge-Ge contacts at all compositions. A further refinement is multiedge fitting, which permits simultaneous analysis from two different ''perspectives'' (core edges of different atoms), allowing for more constraints in the fitting. In this case, we require the fits to the Si-*K* and Ge-*K* XAFS data for a given composition to have an identical SiGe bond length and associated Debye-Waller parameter. A third level of constrained fitting is to optimize fit parameters based on some assumed functional relationship among the structural parameters, for example requiring a linear relationship of the compositional variation of $\mathbf{r}_{\mathrm{GeGe}}$, $\mathbf{r}_{\mathrm{SiGe}}$, and $\mathbf{r}_{\mathrm{SiSi}}$ bond lengths, and fitting the three slopes and intercepts instead of the individual bond lengths. This last approach was explored but abandoned, since it assumes the functional form of the compositional dependence, which is something we are trying to determine in this paper.

The structural models for the FEFF calculations consisted of >100 atom cluster models of: the Si lattice for the Si-Si distance, the Ge lattice for the Ge-Ge distance, and a single Ge (Si) atom in a Si (Ge) lattice as the model for the Ge-Si and Si-Ge pairs. Twenty data sets were fit simultaneously. There were a total of 69 independent variables in the fit, which meant that the data set was not over determined (standard methods indicate there are 270 independent points[12]). The Feffit constraints imposed were: (i) same $R_{\text{Si-Ge}}$ for the same composition alloy in both Si *K*-edge and Ge *K*-edge XAFS; (ii) constant E_0 for each type of atom pair (Si-Si, Si-Ge; Ge-Si, and Ge-Ge); (iii) same Debye-Waller (DW) parameter for each type of atom pair (Si-Si, Si-Ge; Ge-Si, and Ge-Ge), except for the 56% alloy, which was treated differently because of suspected higher static disorder. The data for pure *c*-Si and *c*-Ge was included in the fit to help establish correct E_0 and DW values by constraining the interatomic distances and coordination numbers to the well-known crystallographic values. Uncertainties in the final results are those reported by Feffit. The final first-shell structural results are summarized in Table III for both the relaxed samples, fit simultaneously to explore the thermodynamic limit, and for a selection of strained samples, investigated to determine the sensitivity of high quality XAFS to the effects of epitaxial strain on first-shell bond lengths in SiGe alloys.

B. Structural results

Figure 5 shows the final optimized fits to the Fourier-filtered Ge and Si *K*-edge data. Aside from the result for the Si 1*s* data for sample *S*42*r*, there is excellent match between the XAFS calculated using the optimized parameters and the experimental Fourier-filtered XAFS. The Si *K*-edge data for *S*42*r* was the worst of those for the relaxed samples and it is possible the short range, combined with distortions related to incompletely suppressed diffraction glitches could be the cause of the anomalously poor fit in this case.

Several checks have been made to test the consistency of the results with other structural information known about crystalline SiGe alloys. Figure 6 compares the XAFS first-shell coordination numbers with those predicted from the sample composition derived from x-ray diffraction assuming random site occupancy. The coordination number results are

TABLE III. Results of fit of Fourier-filtered first-shell XAFS signal of crystalline SiGe alloys using Feffit.

		Si-Si		Si-Ge			Ge-Ge	
Code	%Si (target)[a]	R (Å)	N-Si	R (Å)	N-Ge	N-Si	R (Å)	N-Ge
c-Ge	0 (Ge x11)						2.450	4.00
$G5s$	5 (5)	b	b	2.408 (8)	3.5 (4)	c	c	c
$G9r$	9 (10)	b	b	2.398 (15)	3.7 (8)	c	c	c
$G12s$	12 (12)	b	b	2.400 (9)	3.9 (5)	c	c	c
$G20s$	20 (20)	b	b	2.407 (14)	3.2 (8)	c	c	c
$G22s$	22 (22)	b	b	2.407 (20)	3.1 (9)	c	c	c
$S29r$	29 (25)	2.367 (55)	1.2 (5)	2.415 (7)	3.5 (7)	1.13 (7)	2.438 (2)	3.56 (7)
$G38r$	38 (30)	2.354 (32)	1.2 (3)	2.397 (10)	2.2 (4)	<0.2	c	c
$S42r$	42 (40)	2.351 (34)	1.9 (5)	2.388 (5)	2.7 (7)	1.64 (7)	2.439 (3)	2.40 (9)
$S56r$	56 (50)	2.354 (17)	2.2 (4)	2.395 (7)	1.7 (4)	2.16 (25)	2.432 (9)	2.22
$S61r$	61 (60)	2.355 (13)	2.4 (2)	2.388 (5)	1.7 (3)	2.35 (7)	2.435 (4)	1.52 (7)
$S78r$	78 (75)	2.369 (10)	3.3 (2)	2.389 (5)	1.3 (3)	3.47 (13)	2.395 (10)	1.24
$S91s$	91 (90)	2.350 (9)	3.2 (2)	2.388 (3)	0.6 (2)	3.55 (14)	b	b
$S99s$	99.2 (99.2)			b	b	b	2.396 (8)	3.4 (3)
c-Si	100 (Si x11)	2.352	4.00					

[a]Values quoted (and used in plots etc) are from x-ray diffraction-based compositional analysis. The values in brackets were the target compositions during growth.

[b]System was too dilute in this component for reliable identification of the signal.

[c]Ge-dilute samples on Ge susbtrates could not be measured due to substrate interference.

in good agreement with random site occupancy. A second consistency check involves comparing XAFS-predicted and measured lattice parameters. For a random solid solution with a diamond cubic lattice the lattice parameter $a = 4*\langle \mathbf{r} \rangle/3$, where $\langle \mathbf{r} \rangle = (1-x)^2 r_{GG} + x^2 r_{SS} + 2x(1-x) r_{GS}$, x is the %Si, and r_{GG}, r_{SS}, and r_{GS} are the atom pair bond lengths. Figure 7 plots the lattice parameter derived from the XAFS coordination numbers and bond lengths as a function of the composition (determined by the x-ray diffraction lattice constant), with the compositional variation of the lattice constant obtained from x-ray diffraction.[9] A dotted line to indicate perfect Vegard behavior is also plotted. The dashed line indicates the predicted lattice parameter based on topological rigidity model parameters of $\mathbf{a}^{**} = 0.70$, 0.84, and 0.94, the values derived from linear fits to the first-shell XAFS data (see below). The XAFS results are consistent with the crystallographic lattice parameters within the error

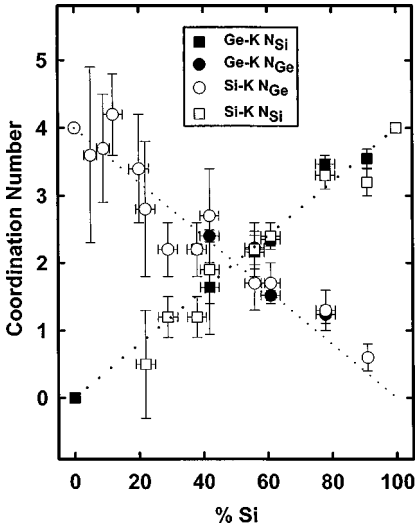

FIG. 6. Coordination numbers derived from XAFS as a function of composition. The dotted lines indicate the coordination numbers predicted from x-ray diffraction assuming random site occupancy.

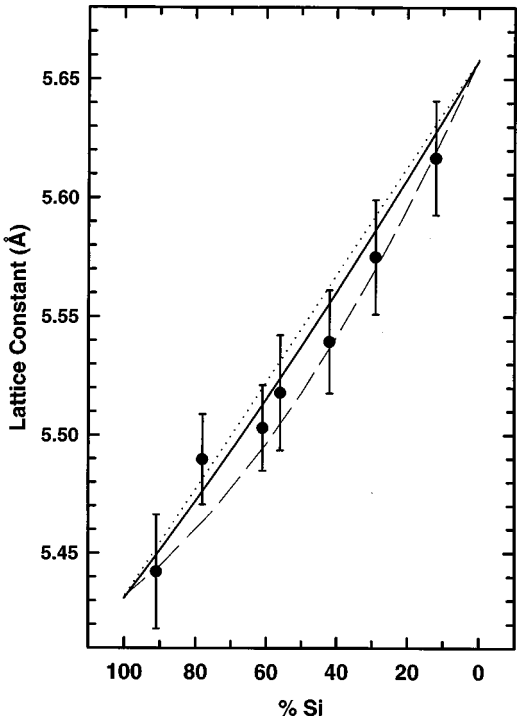

FIG. 7. Lattice parameter derived from XAFS first-shell coordination numbers and bond distances as a function of sample composition, %Si. The solid line is the lattice parameter from crystallography[9] while the dotted line is the Vegard model prediction. The dashed line indicates the predicted lattice parameter based on topological rigidity model parameters of $\mathbf{a}^{**} = 0.70$, 0.84, and 0.94 for the Ge-Ge, Si-Ge, and Ge-Ge bonds, the values derived from linear fits to our data.

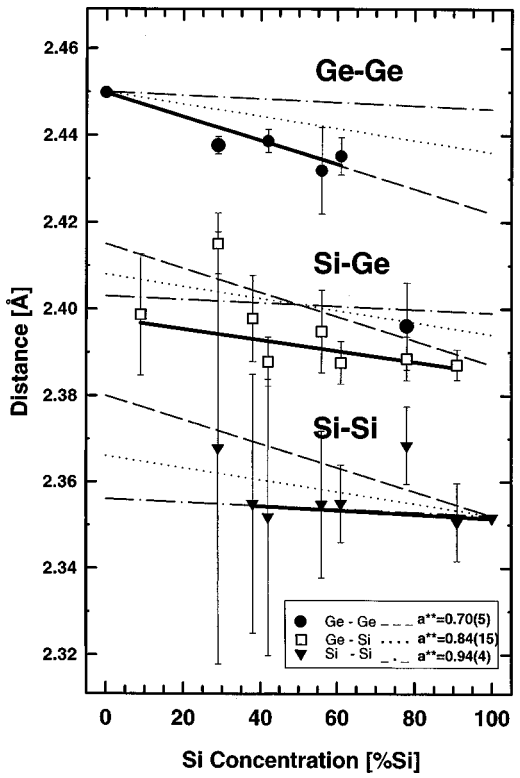

FIG. 8. First-shell bond lengths derived from multifile analysis. The bold fit lines are a linear least squares fit to the data (excluding the $Si_{25}Ge_{75}$ and $Si_{78}Ge_{22}$ points). The dash, dot, and dash-dot lines are the predicted compositional-dependence of the bond lengths within the topological rigidity model for a^{**} values of 0.70(5), 0.84(15), and 0.94(4), respectively. These values are those which match the slope of the Ge-Ge, Ge-Si, and Si-Si linear least squares fit lines.

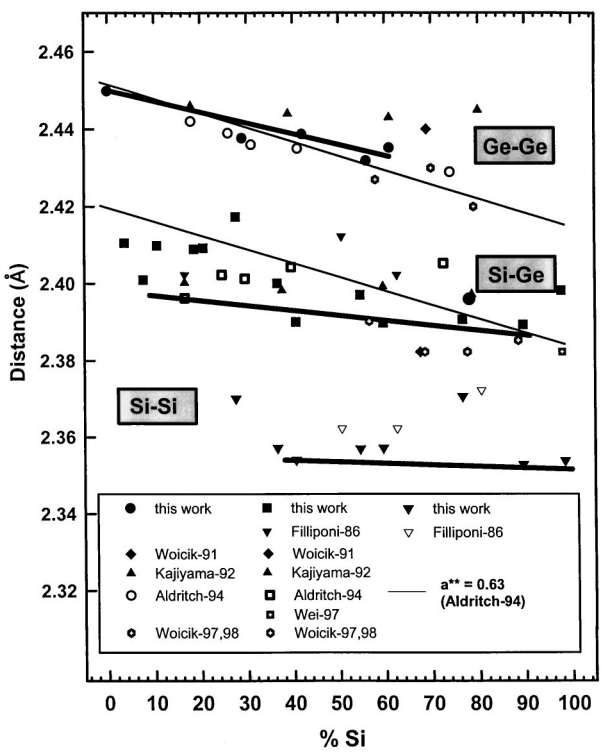

FIG. 9. Comparison of the present results to experimental and theoretical values reported in the literature (Refs. 21–30)—see legend for correlation of symbols with first authors of the literature reports.

bars; in particular, they reproduce (and perhaps over estimate) the known, slight negative deviation from Vegard's law.[8]

Figure 8 plots the derived Ge-Ge, Ge-Si, and Si-Si bond lengths as a function of alloy composition. The dark solid lines are linear regression lines. [Note that the data for the samples near 25% and 75% Si (*S*29*r*, *S*78*r* codes) were not included in the linear fit since we believe there may be distortions due to compound formation around these compositions—see below]. Our results are inconsistent with the topological rigidity model,[16–19] since that model requires similar slopes of the $R(x_{Si})$ lines for the Ge-Ge, Si-Ge, and Si-Si pairs. Application of this framework[16–18] gives a^{**} values of 0.70(5), 0.84(15), and 0.94(4) based on the slopes of the linear fits to the Ge-Ge, Ge-Si, and Si-Si data, respectively. Lines corresponding to these three a^{**} values are indicated in Fig. 8. The a^{**} value of 0.70(5) derived from our Ge-Ge values is close to that of 0.63(10) reported by Aldrich *et al.*[29] However, our results are a significant extension of the Aldrich *et al.* work since we have determined $\mathbf{r}_{SiSi}$, $\mathbf{r}_{SiGe}$, and $\mathbf{r}_{GeGe}$ in a consistent manner and we have shown that the differences in the compositional variation of the $\mathbf{r}_{SiSi}$ and $\mathbf{r}_{GeGe}$ are outside the mutual error bars. The observation of a significant variation in $\mathbf{r}_{SiGe}$ is also noteworthy since the $\mathbf{r}_{SiGe}$ values of Aldrich *et al.*[29] are consistent with a horizontal, Pauling limit line, as well as with their preferred interpretation of a sloped, partial-Vegard limit line.

The average a^{**} (weighted by the number of data points for each *R* type) is 0.84(12), considerably larger than the values of 0.63–0.75 determined by other theoretical[8,16–20] and experimental[29] studies. Note however, this average is rather meaningless since the slopes of the three different $R(x)$ data are different and thus the topological rigidity model is not directly applicable. It is also noteworthy that the $\mathbf{r}_{SiGe}$ line for $a^{**}=0.84$ (dotted in Fig. 8) reproduces the *slope* of the $R_{Si\text{-}Ge}(x)$ line but it lies 0.01 Å above all of the Si-Ge values derived from our XAFS measurements. According to the basic assumptions of the topological rigidity model,[16–19] the SiGe distance in a 50% alloy compositions must be the sum of the Si and Ge covalent radii (2.40 Å), whereas we determine Si-Ge distance in alloys around 50% to be well below that value, as has been found in earlier XAFS studies.[27,29]

Figure 9 compares our first-shell bond length results and their associated trend lines with all of the literature experimental XAFS data.[21–30] For this plot, we have not indicated error bars, in part because they were not always reported, and in part, for clarity. We note that this plot incorporates data from amorphous as well as strained and relaxed crystalline Si-Ge alloys. Figure 9 also plots our best estimate of the linear trend lines derived from the internally consistent analysis of our data (i.e., the solid lines from Fig. 8), as well as the line for $a^{**}=0.63(10)$ reported by Aldrich *et al.*[29] While there is some evidence from our work, as well as that of Woicik *et al.*[26,27] that XAFS may reflect first-shell structural differences in strained and relaxed crystalline alloys of the same nominal composition, one simple interpretation of Fig. 9 is that all of the data are showing generally the same trends, with a scatter about the mean trend line of ± 0.01 Å.

This is well within the generally accepted accuracy of ± 0.02 Å for a single-sample XAFS analysis, although our experience with using XAFS in a comparative sense with simultaneous constrained fitting of a series of related samples is that uncertainties below ± 0.01 Å are possible with good data and good models.

IV. DISCUSSION

Our results for the relaxed single-crystal SiGe alloys (Fig. 8) indicate that the Si-Si bond length is only weakly dependent on composition, whereas there is a significant change in the Si-Ge bond length and an even larger change in the Ge-Ge bond length. Overall our results imply that the bonding in crystalline SiGe alloys is rather close to the Pauling limit, in agreement with most earlier XAFS studies. Most of the strain in SiGe alloys must be accommodated by bond angle rather than bond length changes, in agreement with the conclusion of other studies.[39] However, the extent of Pauling behavior depends on the bond type. Naively one might expect the Ge-Ge distance to be less adaptable than the Si-Si distance to a changing environment since Ge is the larger atom and thus, in a close packing model, should determine the lattice. However, for the pure materials, the Debye temperature of Si is significantly higher than that for Ge, consistent with a stiffer bond. Perhaps differences in the pairwise electronic interactions controls the bond length—composition trend, more than space-filling considerations.[26,27]

Exceptions to the general trends are (i) a noticeably shorter Ge-Ge bond length in Si-rich alloys (the *S*78*r* sample), and (ii) slightly off-trend values for compositions around $SiGe_3$ and Si_3Ge. While the scatter in the full analysis is such that the deviation at these compositions from the trend is marginally statistically significant, we find that there is a clear change in the XAFS frequency when one compares $\chi(k)$ and $F(R)$ data for these compositions in comparison to the data for a closely adjacent alloy. For example the value determined for the sample of 78% Si composition for $\mathbf{r}_{\text{Ge-Ge}}$ is ~ 0.04 Å smaller than that for the 61% Si sample, while the value determined for $\mathbf{r}_{\text{Si-Si}}$ for 78% Si is ~ 0.02 Å larger than that for the 61% Si sample. Figure 10 compares raw and first-shell Fourier-filtered Si *K*-edge XAFS for the 61% and 78% samples. The reduced XAFS periodicity, and the accompanying shift of the Fourier-transform peak to larger *R* in the 78% sample, reflect a marked change in the Si-Si distance since the Si-Si XAFS contribution dominates Si *K*-edge XAFS at these compositions. We present this as strong evidence that the change in the bond length between these two compositions is larger than that expected from the trend exhibited in Fig. 8. The ''anomalous one'' is that closer to the Si_3Ge composition. Although further study is clearly needed, the intriguing possibility exists that these deviations from the general trends are evidence for some tendency toward compound formation at specific composition ranges.

Looking more closely at the $\mathbf{r}_{\text{GeGe}}$ results in Fig. 8, there is also evidence that the compositional dependence of the bond lengths is nonlinear at the impurity limits. At very low-Ge concentrations (high x_{Si}) the Ge-Ge contact corresponds to a dimer in a relatively unperturbed Si host lattice. If the linear fit to the central part of Fig. 8 is extrapolated, the

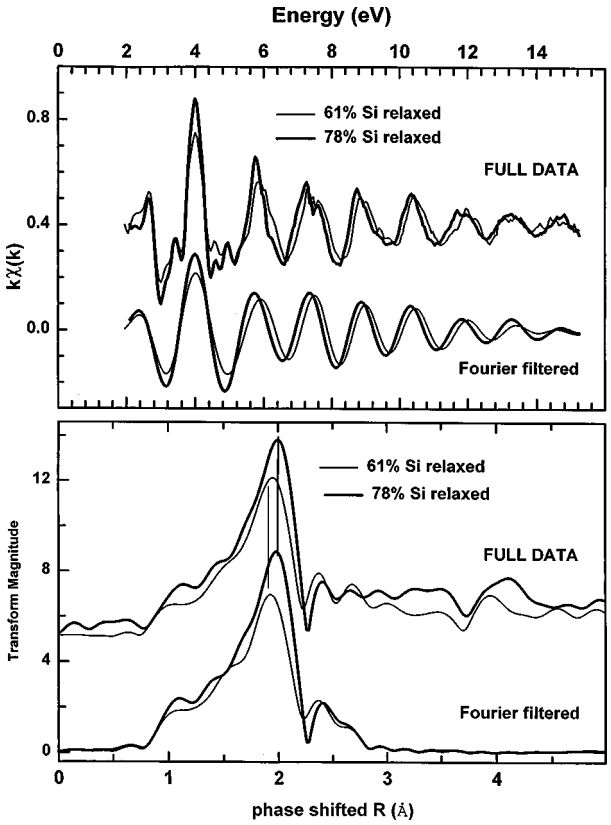

FIG. 10. Raw and first-shell Fourier-filtered $\chi(k)$ and $F(R)$ signals for $Si_{61}Ge_{39}$ and $Si_{78}Ge_{22}$ alloys. The shift in XAFS frequency and shift in the magnitude of the Fourier-transform peak is evidence for an anomaly in the structure around the Si_3Ge composition. Similar, though less dramatic, changes were observed for compositions around 30% Si.

Ge-Ge bond length for $Si_{0.8}Ge_{0.2}$ should be about 2.43 Å, whereas the Ge-Ge distance derived from the XAFS of sample *S*78*r* is less than 2.40 Å. It is possible that the surrounding Si lattice constrains the Ge-Ge bond length of the isolated Ge-Ge dimer to a shorter value than the natural Pauling-limit Ge-Ge distance. Although Martins and Zunger[8] calculated heteroatomic bond lengths for single atomic impurities (Ge in a Si host lattice) there are no calculations for the structure of isolated dimers. Weidmann and Newman[15] have performed modeling studies of bond-length distributions in alloys at the dilute limits, and their results indicate that the distributions are highly complex, i.e., far from the Gaussian-shaped distribution predicted by the theory of Thorpe and colleagues. Wei *et al.*[30] have recently used XAFS to study the environment of ultradilute Ge in Si ($Si_{0.994}Ge_{0.006}$) and report $\mathbf{r}_{\text{GeSi}} = 2.38(1)$ Å, as opposed to our result, 2.396(8) Å (*S*99*s*). The discrepancy is just outside of the mutual error bars, and it is unlikely to be related to strain since this will have only a very small effect at this level of dilution. In general, Ge-Ge bond length at the dilute limit seems to be a very interesting area for further study.

The SiGe system is often used as an example of a near-ideal solution, since Si and Ge are 100% miscibile and since Vegard's law is approximately correct.[40] However, recent work has shown that SiGe materials grown by nonequilibrium methods such as MBE or CVD, may not be as ideal as the thermodynamic equilibrium bulk material. Specifically,

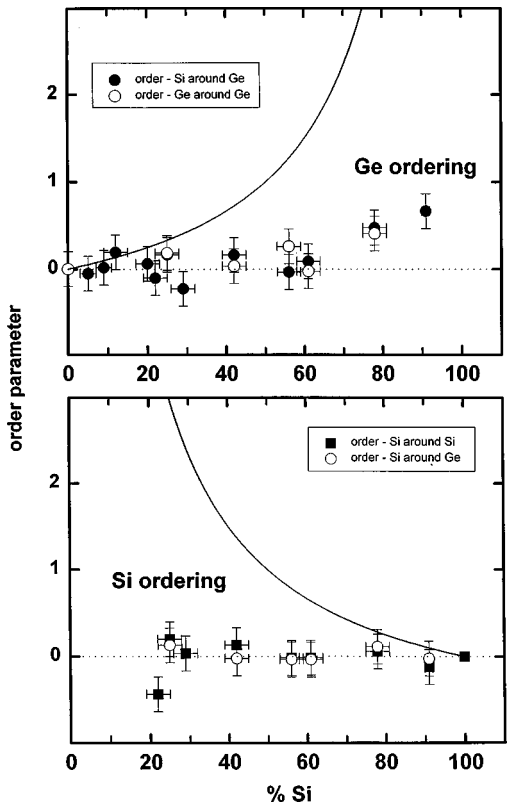

FIG. 11. Test of ordering from coordination number analysis. The deviation of the Ge order parameter at large %Si is an indication of Ge-Ge clustering. See text for further details.

published results by a large number of groups seem to indicate that thin film SiGe alloys may have *ordered* regions.[41–50] The specific nature of the ordered regions is still a subject of lively debate; however, it seems clear that the ordering is a result of kinetics and strain, and not thermodynamics.[14,45] Tentative structural models for the ordering include CuPt- and CuAu-*I*-type ordering,[49] where Ge-Ge and Si-Si dimers are preferentially arranged on various planes. If significant ordering is present in these MBE-grown SiGe alloys, the Ge *K*-edge XAFS results, particularly the coordination numbers, would be significantly affected. For example, ordering of Ge into dimers in the 91% Si alloy would increase the amount of Ge-Ge coordination from that of a truly random alloy, which might be detectable by XAFS. Additionally, some of the structural models proposed in the literature involve large microscopic strains.[49] This could affect local bond lengths determined from Ge *K*-edge XAFS.

Diffraction studies of these and closely related samples grown in the same MBE chamber indicate there is evidence for ordering.[49] We have explored the sensitivity of our XAFS results to this ordering by evaluating $\Gamma_{A\text{-}B}$, the order parameter devised by Cargill and Spaepen.[51] For SiGe alloys, where each atom is four coordinate, $\Gamma_{A\text{-}B}=(0.25N_G-x)/x$. For a completely random alloy, the fraction of a given atom around a central atom is equal to that predicted by the composition, and $\Gamma_{A\text{-}B}$ is zero. Nonzero values of $\Gamma_{A\text{-}B}$ indicate ordering. Figure 11 depicts the order parameter calculated for both Ge and Si ordering from our Si and Ge *K*-edge fit results, along with curves for the cases of complete randomness and perfect order. The error bars for the value of the order parameter were assigned to be ± 0.2, which is larger than those based on the statistical errors in the coordination numbers, but in better agreement with data scatter. The comparison of order parameters for high-% Si alloys derived from Ge *K*-edge results relative to those of Si *K*-edge results is quite interesting. In Fig. 11(a), it seems that in the low-Ge limit, Ge is preferentially coordinated to itself, rather than with Si, suggesting dimer formation. The corresponding plot for Si ordering, Fig. 11(b), indicates there is no preference for Si-Si dimer formation in Ge-rich alloys. The suggestion of Ge selfcoordination is a surprising result, but one which might be real given that it is indicated by coordination numbers derived from both Si and Ge *K*-edge XAFS.

A. Strained SiGe alloys

Most of the samples analyzed in the preceding sections were ones where the material was grown far beyond the upper thickness for strained systems and thus it is spontaneously relaxed in growth, or, in a few cases, has been annealed to ensure the relaxed, thermodynamically most stable structure. However, the material used in SiGe devices[1–3] is grown to a thickness less than that where it should spontaneously relax, and thus it is typically in a metastable strained state. Epitaxial strain accommodation at the atomic level is a subject of enormous importance in materials growth, and not surprisingly there has been considerable studies of strained crystalline semiconductors, particularly III-V systems.[52–54] Understanding and controlling the geometry of SiGe through epitaxial strain has great potential for producing advances in SiGe device engineering. Thus, there is considerable impetus to extend these types of measurements to fully strained layers. We have investigate the Si 1*s* and Ge 1*s* XAFS of a number of strained crystalline SiGe alloy samples. In general the differences from the relaxed counterparts of the same composition are too small to be documented, although in a few cases there was evidence for measurable differences. Clearly identifying first-shell bond-length changes associated with strain in SiGe crystalline alloys is at the limits of the precision of XAFS.

In general, strained epilayers on Si present considerable problems for Si *K*-edge XAFS measurements, because they are so thin. As the thickness decreases, the TEY signal of the epilayer is contaminated by that of the substrate. FY is not practical unless total external reflection conditions are established. Though substrate contamination is less of a problem for studies of Si *K*-edge measurements of strained SiGe alloys grown on Ge, the critical thickness of SiGe epilayers on Ge is substantially lower than that for epilayers on Si. This introduces problems with weak signal and thus poor signal-to-noise ratio. In order to avoid substrate interference in Ge *K*-edge measurements it is essential to work at grazing incidence, preferably below the external reflection angle, as has been reported recently by Oyanagi *et al.*[55,56]

Another way to address the question of strain accommodation in SiGe at the local level would be to perform a detailed second shell analysis of the data.[18,27,57] There are six unique second-shell distances that the topological rigidity model predicts vary by approximately 0.07 Å over the entire composition range.[18] This is much larger than the ~0.02 Å variation of the first-shell distances. Second-shell analysis permits development of a short range lattice model of the

SiGe structure, which could then determine both bond-length and bond-angle accommodation of strain. However, second-shell analysis is a difficult task since the second-shell signal strongly overlaps the third-shell signal and is heavily contaminated by a triangular multiple scattering path. In addition, because of the random substitutional nature of the structure, the spread in second-shell bond lengths is effectively a large static disorder term, which makes it very difficult to identify this signal component. Nevertheless, Woicik *et al.*[27] have recently reported such a polarization dependent two-shell analysis for Ge *K*-XAFS of strained $Si_{0.78}Ge_{0.21}$ and find that the first- and second-shell signal can only be interpreted simultaneously if $R_{GeGe}=2.43(2)$ Å and $R_{Ge\text{-}Si}=2.38(2)$ Å. Interestingly, Chen *et al.*[58] have used photoelectron diffraction to study the initial stages of the growth of Ge on Si(001) and they report a Ge-Ge bond length in this highly strained environment of 2.43(10) Å. Oyanagi *et al.*[56] also report that the Ge-Ge distance for the first layer of Ge on Si(001) is very long—indeed they report $r_{GeGe}=2.51(4)$ Å, longer than the relaxed Ge-Ge bond length in *c*-Ge! These results for Ge-Ge distances in a strained environment are rather surprising given that the stress imposed by commensurate epitaxial growth of Ge on Si should lead to an anomalously short Ge-Ge bond length, in the limit approaching the value of 2.35 Å for the Si-Si substrate. It is certainly noteworthy that all of these values are *significantly off our curves*. Strain in SiGe may have large effects on the Ge-Ge distance in Ge_2 dimers that occur in dilute Ge in Si systems.

B. Comparison to XAFS of other alloy systems

How do our results for relaxed crystalline SiGe alloys compare to those for other alloy systems? XAFS studies have been performed on a wide range of metallic, insulating, and semiconducting alloys. Boyce and Mikkelson[59] found that the highly covalent (In,Ga)As system is very Pauling-like (Cai and Thorpe[18] calculate $\mathbf{a}^{**}=0.80$). Sasaki *et al.*[60] found similar bonding, but with more lattice rigidity (more VCA-like) for another III-V alloy, Ga(As,P) ($\mathbf{a}^{**}=0.63$ from there results). Much more ionic materials, such as the II-VI compounds, (Zn,Mn)Se, (Zn,Cd)Te, and (Cd,Mn)Te have been shown to have Pauling-dominated bonding with $\mathbf{a}^{**}=0.80$, 0.82, and 0.90, respectively.[61–63] Even purely ionic materials have demonstrated mixed-type behavior, as evidenced by the results for (*K*,Rb)Br and Rb(Br,*I*) where $\mathbf{a}^{**}=0.52$ and 0.64, respectively.[64] Thus, the highly, but not completely, Pauling-type structure of SiGe alloys is typical of a wide range of semiconductor alloys. Frenkel *et al.*[65] have studied Cu *K*- and Au *L*-edges XAFS of metastable CuAu alloys and have used a multifile, multiedge analysis similar to that employed in this study. They found significant mixed-type behavior, with the Au-Au, Cu-Au, and Cu-Cu bond lengths all showing measurable dependence upon composition, much as in SiGe and other semiconductor systems. However, Frenkel *et al.*[65] suggested that the Au atoms in the alloy form a long-range network (i.e., ''cage'') that essentially determines the lattice parameter of the alloy. The Cu atoms, being much smaller, fit into the ''holes'' in the Au ''cage''. Thus, $\mathbf{r}_{AuAu}$ was found to be less dependent upon composition than $\mathbf{r}_{CuAu}$ and $\mathbf{r}_{CuCu}$. In support of this model, the authors found from their fitting results that the σ^2_{CuCu} and σ^2_{CuAu} values were significantly larger than that of σ^2_{AuAu}. From these results, Frenkel *et al.*[65] questioned the general applicability of theories based on elastic properties of the sample[26,27] to all systems. Our present results support this viewpoint, although in our case it is the distance between the larger Ge atoms that shows the largest change with composition.

V. SUMMARY

High-quality Si and Ge *K*-edge XAFS spectra of relaxed crystalline SiGe alloys with a wide range of compositions have been measured and the first-shell signal analyzed using simultaneous, constrained, curve fitting of multiple spectra/samples. The compositional dependence of the first-shell homoatomic and heteroatomic bonding in SiGe alloys has been found to be mostly, but not completely, Pauling-type in nature. This is in good agreement with most previous XAFS studies[21–29] but in disagreement with essentially all published theoretical results[8,13–18,20] that propose a systematic linear variation that is (a) similar in slope for the SiSi, SiGe, and GeGe bond lengths, and (b) produces changes in bond length of ~0.03 Å over the full composition range. A more extensive XAFS study of low-composition alloys, as well as theoretical work, would permit better exploration of nonlinear effects expected with isolated impurity dimers.

ACKNOWLEDGMENTS

This work has been financially supported by NSERC (Canada). The CHESS and SRC synchrotron radiation facilities are funded by NSF under Contracts Nos. DMR-9311772 and DMR 95-31009. We thank the staff of these facilities for their assistance and expert operation and maintenance of the facilities.

[1] U. Konig and H. Dambkes, Solid-State Electron. **38**, 1595 (1995).
[2] J. C. Bean, Proc. IEEE **80**, 571 (1992).
[3] T. P. Pearsall, Mater. Sci. Eng., B **9**, 225 (1991).
[4] H. Stohr and W. Klemm, Z. Anorg. Allg. Chem. **241**, 313 (1939).
[5] R. W. Olesinski and G. J. Abbaschian, Bull. Alloy Phase Diagrams **5**, 227 (1984).
[6] Q. M. Ma, K. L. Wang, and J. N. Schulman, Phys. Rev. B **47**, 1936 (1993).
[7] C. A. King, J. L. Hoyt, C. M. Gronet, J. F. Gibbons, M. P. Scott, and J. Turner, IEEE Electron Device Lett. **10**, 2323 (1989).
[8] J. L. Martins and A. Zunger, Phys. Rev. B **30**, 6217 (1984); Phys. Rev. Lett. **56**, 1400 (1986).
[9] P. Dismukes, L. Ekstrom, and R. J. Paff, J. Phys. Chem. **68**, 3021 (1964); E. Kasper, J. Cryst. Growth **150**, 921 (1995).
[10] L. Pauling, *The Nature of the Chemical Bond* (Cornell University Press, Ithaca, NY, 1967).
[11] P. A. Lee, P. H. Citrin, P. Eisenberg, and B. M. Kincaid, Rev. Mod. Phys. **53**, 769 (1981).
[12] *X-Ray Absorption: Principles, Applications, Techniques of EXAFS, SEXAFS, and XANES*, edited by D. C. Konigsberger

and R. Prins (Wiley, Toronto, 1988).
[13] M. Ichimura, Y. Nishino, H. Kajiyama, and T. Wada, Jpn. J. Appl. Phys., Part 1 **29**, 842 (1990).
[14] S. de Gironcoli, P. Giannozzi, and S. Baroni, Phys. Rev. Lett. **66**, 2116 (1991).
[15] M. R. Weidmann and K. E. Newmann, Phys. Rev. B **45**, 8388 (1992).
[16] Y. Cai and M. F. Thorpe, Phys. Rev. B **46**, 15 872 (1992).
[17] Y. Cai and M. F. Thorpe, Phys. Rev. B **46**, 15 879 (1992).
[18] N. Mousseau and M. F. Thorpe, Phys. Rev. B **46**, 15 887 (1992).
[19] J. G. Kirkwood, J. Chem. Phys. **7**, 506 (1939).
[20] N. Mousseau and M. F. Thorpe, Phys. Rev. B **48**, 5172 (1993).
[21] L. Incocia, S. Mobilio, M. G. Proietti, P. Fiorini, C. Giovannella, and F. Evangelisti, Phys. Rev. B **31**, 1028 (1985).
[22] A. Filliponi, P. Fiorini, F. Evangelisti, A. Balerna, and S. Mobilio, J. Phys. (Paris), Colloq. **8**, 357 (1986).
[23] Y. Nishino, S. Muramatsu, Y. Takano, and H. Kajiyama, Phys. Rev. B **38**, 1942 (1988).
[24] M. Matsuura, J. M. Tonnerre, and G. S. Cargill, Phys. Rev. B **44**, 3842 (1991).
[25] J. C. Woicik, C. E. Bouldin, M. I. Bell, J. O. Cross, D. J. Tweet, B. D. Swanson, T. M. Zhang, L. B. Sorenson, C. A. King, J. L. Hoyt, P. Pianetta, and J. F. Gibbons, Phys. Rev. B **43**, 2419 (1991).
[26] J. C. Woicik and C. E. Bouldin, Phys. Rev. B **55**, 15 386 (1997).
[27] J. C. Woicik, K. E. Miyano, C. A. King, R. W. Johnson, J. G. Pellegrino, T.-L. Lee, and Z. H. Lu, Phys. Rev. B **57**, 14 592 (1998).
[28] H. Kajiyama, S. Muramatsu, T. Shimada, and Y. Nishino, Phys. Rev. B **45**, 14 005 (1992).
[29] D. B. Aldrich, R. J. Nemanich, and D. E. Sayers, Phys. Rev. B **50**, 15 026 (1994).
[30] S. Wei, H. Oyanagi, H. Kawanami, K. Sakamoto, T. Sakamoto, K. Tamura, N. L. Saini, and K. Uosaki, J. Appl. Phys. **82**, 4810 (1997).
[31] A. P. Hitchcock, T. Tyliszczak, P. Aebi, J. Z. Xiong, T. K. Sham, K. M. Baines, K. A. Muller, X. H. Feng, J. M. Chen, B. X. Yang, Z. H. Lu, J.-M. Baribeau, and T. E. Jackman, Surf. Sci. **291**, 349 (1993).
[32] A. P. Hitchcock, T. Tyliszczak, P. Aebi, X. H. Feng, Z. H. Lu, J.-M. Baribeau, and T. E. Jackman, Surf. Sci. **301**, 260 (1994).
[33] T. Tyliszczak, A. P. Hitchcock, Z. H. Lu, J.-M. Baribeau, and T. E. Jackman, Scanning Microsc. **8**, 795 (1994).
[34] T. Tyliszczak and A. P. Hitchcock, Physica B **158**, 335 (1989).
[35] A. Erbil, G. S. Cargill III, R. Frahm, and R. F. Boehme, Phys. Rev. B **37**, 2450 (1988).
[36] J. J. Rehr, J. Mustre de Leon, S. I. Zabinsky, and R. C. Albers, Phys. Rev. B **44**, 4146 (1991).
[37] S. I. Zabinsky, J. J. Rehr, A. Ankudinov, R. C. Albers, and M. J. Eller, Phys. Rev. B **52**, 2995 (1995).
[38] E. A. Stern, M. Newville, B. Ravel, Y. Yacoby, and D. Haskel, Physica B **208&209**, 117 (1995).
[39] Z. H. Lu, J. M. Baribeau, and T. E. Jackman, Can. J. Phys. **70**, 799 (1992).
[40] A. Ourmazd and J. C. Bean, Phys. Rev. Lett. **55**, 765 (1985).
[41] P. B. Littlewood, Phys. Rev. B **34**, 1363 (1986).
[42] D. J. Lockwood, K. Rajan, E. W. Fenton, J. M. Baribeau, and M. W. Denhoff, Solid State Commun. **61**, 465 (1987).
[43] F. K. LeGoues, V. P. Kesan, and S. S. Iyer, Phys. Rev. Lett. **64**, 40 (1990).
[44] E. Muller, H. U. Nissen, K. A. Mader, M. Ospelt, and H. von Kanel, Philos. Mag. Lett. **64**, 183 (1991).
[45] D. E. Jesson, S. J. Pennycook, and J. M. Baribeau, Phys. Rev. Lett. **66**, 750 (1991).
[46] D. J. Lockwood and J. M. Baribeau, Phys. Rev. B **45**, 8565 (1992).
[47] D. E. Jesson, S. J. Pennycook, J. M. Baribeau, and D. C. Houghton, Phys. Rev. Lett. **68**, 2062 (1992).
[48] D. E. Jesson, S. J. Pennycook, J. Z. Tischler, J. D. Budai, J. M. Baribeau, and D. C. Houghton, Phys. Rev. Lett. **70**, 2293 (1993).
[49] J. Z. Tischler, J. D. Budai, D. E. Jesson, G. Eres, P. Zschack, J. M. Baribeau, and D. C. Houghton, Phys. Rev. B **51**, 10 947 (1995).
[50] N. Ikarashi, A. Oshiyama, A. Sakai, and T. Tatsumi, Phys. Rev. B **51**, 14 786 (1995).
[51] G. S. Cargill and F. Spaepen, J. Non-Cryst. Solids **43**, 91 (1981).
[52] J. C. Woicik, J. O. Cross, C. E. Bouldin, B. Ravel, J. G. Pellegrino, B. Steiner, S. G. Bompadre, L. B. Sorensen, K. E. Miyano, and J. P. Kirkland, Phys. Rev. B **58**, R4216 (1998).
[53] J. C. Woicik, J. G. Pellegrino, B. Steiner, K. E. Miyano, S. G. Bompadre, L. B. Sorensen, T.-L. Lee, and S. Khalid, Phys. Rev. Lett. **79**, 5026 (1997); J. C. Woicik, Phys. Rev. B **57**, 6266 (1998); J. C. Woicik, J. A. Gupta, S. P. Watkins, E. D. Crozier, Appl. Phys. Lett. **73**, 1269 (1998).
[54] F. Romanato, D. De Salvador, M. Berti, A. Drigo, M. Natali, M. Tormen, G. Rossetto, S. Pascarelli, F. Boscherini, C. Lamberti, and S. Mobilio, Phys. Rev. B **57**, 14 619 (1998).
[55] H. Oyanagi *Researches of The Electrotechnical Laboratory* (Electrotechnical Laboratory, Tsukuba, 1994).
[56] H. Oyanagi, K. Sakamoto, R. Shioda, Y. Kuwahara, and K. Haga, Phys. Rev. B **52**, 5824 (1995).
[57] Z. Wu, K. Lu, D. Wang, J. Liu, and H. Jiang, Z. Phys. B **99**, 31 (1995).
[58] X. Chen, D. K. Saldin, E. L. Bullock, L. Patthey, L. S. O. Johanasson, J. Tani, T. Abukawa, and S. Kono, Phys. Rev. B **55**, R7319 (1997).
[59] J. B. Boyce and J. C. Mikkelsen, Jr., Phys. Rev. B **28**, 7130 (1983).
[60] T. Sasaki, T. Onda, R. Ito, and N. Ogasawara, Jpn. J. Appl. Phys., Part 1 **25**, 231 (1985).
[61] A. Balzarotti, N. Motta, A. Kisiel, M. Zimnal-Starnawska, M. T. Czyzyk, and M. Podgorny, Phys. Rev. B **31**, 7526 (1985).
[62] W. F. Pong, R. A. Mayanovic, B. A. Bunker, J. K. Furdyna, and U. Debska, Phys. Rev. B **41**, 8440 (1990).
[63] A. Balzarotti, in *Ternary and Multinary Compounds*, edited by D. S. Deb and A. Zunger (Materials Research Society, Pittsburgh, 1987), p. 333.
[64] J. B. Boyce and J. C. Mikkelsen, Jr., Phys. Rev. B **31**, 6903 (1985).
[65] A. I. Frenkel, E. A. Stern, A. Rubshtein, A. Voronel, and Yu. Rosenberg, J. Phys. IV **C2**, 1005 (1997).